Preprint
UCRL-JC-151896

Interdiffusion in Ni/CrMo Composition-Modulated Films

A.F. Jankowski, C.K. Saw

This article was submitted to
132nd Annual Meeting of The Metallurgical Society
San Diego, CA, March 2-6, 2003

February 18, 2003

U.S. Department of Energy

Lawrence
Livermore
National
Laboratory

Interdiffusion in Ni/CrMo Composition-Modulated Films

Alan F. Jankowski and Cheng K. Saw
Lawrence Livermore National Laboratory, Chemistry and Materials Science
P.O. Box 808, Livermore, CA 94551-9900

Abstract

The measurement of diffusivity at low temperature in the Ni-CrMo alloy system, relative to the melt point, is accomplished through the use of a composition-modulated structure. The composition-modulated structure consists of numerous pairs of alternating Ni and Cr-Mo layers that are each just a few nanometers thick. A direct assessment of alloy stability is made possible through measurement of the atomic diffusion between these layers that occurs during anneal treatments. X ray diffraction under the Bragg condition in the $\theta/2\theta$ mode is the method used to quantify the changes that occur in the short-range order, i.e. the artificial composition fluctuation. The relative intensities of satellite reflections about the Bragg peaks are monitored as a function of the time at temperature. The decay rate of the artificial composition fluctuation of Ni with Cr-Mo is analyzed using the microscopic theory of diffusion to quantify a macroscopic diffusion coefficient $\breve{D}$ as 1.52×10^{-19} $cm^2 \cdot sec^{-1}$ for $Ni_2(Cr,Mo)$ at 760 K.

1. Introduction

The behavior of the Ni-Cr-Mo alloy system is known at high temperatures.[1-5] Aging effects on the microstructure are known in this alloy system, as e.g. in heterogeneous precipitation. The stability of the Ni-22wt.%Cr-13wt.%Mo corrosion-resistant alloy at low temperature can be made by an extrapolation from high temperature data. As an alternative, a direct assessment of stability at temperatures below 800 K is made possible through measurements of the interdiffusion between alternating layers of Ni and Cr-Mo. There is significant interest for the use of this alloy as a containment vessel for the long-term storage of high-level radioactive materials at low temperatures, i.e. less than 500 K.[5] The use of composition-modulated materials, also known as multilayers, is a proven method to examine and control the interdiffusion of materials in samples at low temperatures. For example, the kinetics of spinodal decomposition at temperatures between 473 and 673 K are measured for Cu/Ni and Cu/NiFe composition modulated alloys as prepared by thermal evaporation and sputter deposition methods.[6-8] Quantification of the diffusion kinetics are assessed by analyzing the decay of the nanometric-scaled composition fluctuation using the microscopic theory of diffusion.[6, 9-12]

In this study, Ni/CrMo thin film samples are prepared by magnetron sputter deposition. The growth of the samples along the close-packed planes is anticipated since it has been observed in other face-centered cubic (fcc) and body-centered cubic (bcc) multilayer combinations as Au/Nb.[13] The samples are heat treated to decay the composition profile. An isothermal anneal temperature of 760 K is selected as this temperature is less than the 800 K lower bound normally associated with direct observation of intermetallic phase formation in the Ni-22wt.%Cr-13wt.%Mo, i.e. Ni_2(Cr,Mo) alloy.[1, 4, 5] X-ray diffraction is used to measure the

changes in the composition profile that accompany the heat treatment.[6-8, 12] Three different samples, each of a different composition wavelength, are used to determine the interdiffusivity coefficient ($\check{D}_B$) at each composition wavelength using the microscopic theory of diffusion. The $\check{D}_B$ values are then fit as a function of the composition wavelength for determination of the macroscopic diffusion coefficient ($\check{D}$).[12]

2. Experimental Method

2.1 Sample fabrication

The synthesis of three composition-modulated structures enables an initial study of solid-solution kinetics at low temperature in the Ni-22wt.%Cr-13wt.%Mo alloy. The Ni/CrMo multilayer films are prepared by planar magnetron sputter deposition. The deposition chamber is cryogenically pumped to a base pressure of 1.6×10^{-5} Pa. Three magnetron sources are situated 20 cm beneath the substrate platen. An argon gas pressure of 0.67 Pa, at a mass flow rate of 0.42 $cm^3 \cdot sec^{-1}$, is used to sputter the 6.3 cm diameter targets.

The substrate passes sequentially over each of the targets. Two of the targets are 0.99994 Ni and the third is a composite comprised of a Mo and Cr pieces. For the source-to-substrate distance and the sputter gas parameters used in these depositions, a 2:1 ratio of the Cr to Mo area in the composite target yields a $Cr_{0.65}Mo_{0.35}$ film composition as measured using energy dispersive spectroscopy (EDS). To produce an approximation of the Ni-22wt.%Cr-13wt.%Mo, i.e. $Ni_{0.665}(Cr\text{-}Mo)_{0.335}$, alloy composition in the deposited film, the number of atomic planes of Ni to number of atomic planes of Cr-Mo is held constant at a ratio of 5:3. The thickness of the Ni layer with respect to the layer pair is designated as Γ_{Ni}. EDS analysis of the deposited multilayer films confirms a composition of 64-67 at.% Ni.

The magnetron sources are operated in the dc mode with 100-134 Watt forward power at 260-300 Volt discharges. The instantaneous deposition rates are calibrated to the applied target power using 6MHz quartz crystal microbalances. The deposition rates range from 4.5×10^{-4} to 5.0×10^{-4} nm·W^{-1}·sec^{-1}. To vary the composition wavelength ($d_{Ni/CrMo}$), i.e. the repeat period of the layer pairs, we vary the frequency (ω) of the substrate table rotation and the total number (N) of layer pairs differs for each of three samples to yield a constant film thickness ($N \cdot d_{Ni/CrMo}$) of 1.00 μm. Quartz crystal measurements of $d_{Ni/CrMo}$ and Γ_{Ni} for the three multilayer samples are listed in Table 1. Silicon and sapphire wafers (0.50 mm thick) as well as cleaved mica (0.05-0.10 mm thick) are used for the substrates. A 50 nm buffer of pure Ni is first deposited at the base layer to initiate a (111) fcc Ni growth. The substrate table temperature is 302-319 K during the sputter deposition process.

The sputter deposition parameters for the working gas pressure, source-to-substrate separation, and discharge voltage should ensure that the sputtered neutrals are in a near-thermalized condition when arriving at the substrate.[14-15] The transition from line-of-sight, energetic sputtered neutrals to diffusive thermal atoms occurs beyond a 10 cm traveling distance for a 0.67Pa Ar gas pressure assuming a 350 K gas temperature.

2.2 Heat treatments

The stability of the alloy is assessed through a series of isothermal anneal treatments to progressively homogenize the multilayer films via interdiffusion at each layer interface. The samples are placed within a quartz tube and annealed in a Lindberg™ furnace using an inert atmosphere of flowing Argon gas. The samples are heated to a temperature (T) of 760 ± 12 K at a rate of 0.33 K·sec^{-1}, held at the anneal temperature for a period of time (t), and subsequently

cooled to below 400 K at a rate greater than 2 K·sec^{-1}. Results are presented for samples that are successively pulled from the furnace hot zone at the nominal time intervals 2, 8, and 20 hours.

2.3 X-ray diffraction

The Ni/CrMo multilayer films are characterized with Cu $K\alpha$ x-ray diffraction. A powder diffractometer equipped with a monochromator is operated in the θ/2θ mode over a 2θ range of 20º to 60º. The high-angle diffraction scans reveal the long and short range ordering of the multilayer. The Bragg reflections indicate the film texture whereas the satellite peaks of increasing order (i) reflect the details of the composition modulation in the growth direction. For reference, the interplanar spacing (and 2θ position) of Ni(111), Cr(110), and Mo(110) are 0.2034 nm (44.51º), 0.2040 nm (44.37º), and 0.2225 nm (40.51º), respectively.[16] Each sample is independently measured in the as-deposited condition (t=0) and after the anneal treatment of time interval (t) to facilitate a comparison of the affect of thermal treatment on the composition profile. A Guinier analysis can be applied to calculate the composition profile from the θ/2θ scans since the evolution of the composition profile (beyond the early stages of the anneal treatments) can be routinely fit to a sinusoidal variation.[6, 8, 12]

3. Analysis Method

A quantification of the interdiffusivity is possible by analyzing the decay of a nanometric composition fluctuation, i.e. a static concentration wave, of Ni with Cr-Mo using the microscopic theory of diffusion.[9-12] The advantage of the discrete theory in comparison to the continuous theory is that it can be applied to systems such as ordering, spinodal decomposition, and artificially introduced composition modulation in disordered solutions where the behavior at short wavelengths is of interest. The wavelength, i.e. the repeat periodicity, of the composition

fluctuation ($d_{Ni/CrMo}$) is calculated from the x-ray diffraction scans in the θ/2θ mode by the separation of the satellite reflections about the Ni/CrMo Bragg superlattice reflection.

The satellite peaks reflect the difference in scattering intensity that results from the composition modulation along the growth direction of the sputter deposition film. An asymmetry in the satellite spectrum with enhanced scattering on the low angle side of the fundamental reflection is the result when the modulated solid solution has both widely different scattering factors and atom sizes and if the larger atom has the larger scattering factor.[17] Although asymmetric satellite intensities are the case for alloy systems as Au-Ni, the satellites for the Ni/CrMo multilayer samples should be approximately symmetric as found for the case of Cu/Ni multilayers wherein the component layers have nearly equivalent scattering factors, density, and atomic weight.[6, 8, 16]

The peak intensity $I^i(t)$ of the satellite reflection (i) at each anneal time (t) is defined as normalized to the Bragg reflection $I^B(t)$. The decrease in $I^i(t)$ for the annealed samples from the as-deposited condition of $I^i(0)$ indicates a progressive homogenization of the composition fluctuation with time (t).[6, 9, 11] The satellite intensities are proportional to the square of the composition profile amplitude. The relative decay in satellite intensity determines the amplification factor R(k) as [9-11]

$$\ln\{I^i(t)\cdot[I^i(0)]^{-1}\} = 2R(k)\cdot t. \qquad (1)$$

Typically, the decay of the first-order satellites below and/or above the Bragg reflection (i = -1, +1) are used in the computation of R(k).[6, 12] The amplification factor is related to the generalized interdiffusivity $\check{D}_B$ through the dispersion relationship $B^2(k)$ as [11]

$$R(k) = -B^2(k)\cdot\check{D}_B. \qquad (2)$$

The dispersion relationship $B^2(h)$ for face-centered-cubic (fcc) growth along the [100] or [111] is derived as [11]

$$B^2(h) = 2\{1-\cos(2\pi h)\}\cdot d_{(hkl)}^{-2} \quad (3)$$

where $d_{(hkl)}$ is the (hkl) interplanar spacing of the Bragg reflection,

$$h = d_{(hkl)}\cdot(d_{Ni/CrMo})^{-1}, \quad (4)$$

and

$$d_{Ni/CrMo} = 2\pi k^{-1}. \quad (5)$$

Similarly, derivation of the dispersion relationship $B^2(h)$ for body-centered-cubic (bcc) growth along the [100] or [110] is again expressed by eqn. (3) whereas for [111] growth, the dispersion relationship is given by

$$B^2(h) = 2\{1-\cos^3(2\pi h)\}\cdot\{3d_{(hkl)}^2\}^{-1} \quad (6)$$

The interdiffusivity coefficient(s) $\check{D}_B$ are not only dependent on the dispersion relationship (that accounts for the multilayer periodicity and growth orientation) but also upon temperature (T).

In general, it is customary to assume that there is a linear relationship between ln $\check{D}$ and T^{-1} over a wide range of temperatures, where $\check{D}$ is the bulk diffusion coefficient that is so often measured in a macroscopic diffusion couple. Although it may first appear at long repeat periodicities $d_{Ni/CrMo}$ that $\check{D}_B$ will decrease linearly or inversely proportionate to $B^2(h)$, it is been observed that a higher-order polynomial relationship is useful to fit the behavior of $\check{D}_B$ with $B^2(h)$ especially to account for the behavior at very short composition wavelengths.[6, 12] Thus,

the diffusion coefficient Ď can be related to the interdiffusivity coefficient(s) $Ď_B$ through the expression[12]

$$Ď_B = Ď \cdot \{1 + F_e(h) \cdot (f'')^{-1} + 2(f'')^{-1} \cdot \sum [K_\mu \cdot B^{2\mu}(h)]\} \qquad (7)$$

where $F_e(h)$ is the Fourier transform of the elastic strain energy of the distorted lattice, f'' is the second derivative with respect to composition of the Helmholtz free energy per unit volume, and K_μ are the gradient-energy coefficients. In the long wavelength approximation $-B^2(h)$ equals k^2, and both f'' and K_μ are identical with those expressions appearing in the continuous theories[18-20] or the discrete theory[21]. Eqn (7) describes a general polynomial behavior for the variation of $Ď_B$ with $B^2(h)$ that has a diffusion coefficient defined as Ď. An expansion of the series expression in eqn (7) yields

$$Ď_B = Ď \cdot [1 + K'_1 \cdot B^2(h) + K'_2 \cdot B^4(h) + K'_3 \cdot B^6(h) + \ldots] \qquad (8)$$

where K'_μ equals $2K_\mu \cdot [f'' + F_e(h)]^{-1}$. A plot of $Ď_B$ versus $B^2(h)$ can then be fit with a polynomial curve to determine the diffusion coefficient Ď.

4. Experimental Results and Analysis

The Ni/CrMo multilayer coatings deposited on the sapphire substrates are used in the diffusion analysis. The coatings deposited on the Si substrates evidenced the formation of a nickel silicide as seen in the x-ray diffraction scans even after the initial anneal treatment. The presence of additional Bragg reflections in the diffraction scans interferes with a quantitative assessment of the satellite peak intensities. The coatings deposited on the mica substrates are later intended for the determination of physical properties in the form of free-standing foils. The

coatings deposited on the sapphire substrates did not evidence any change in the baseline diffraction scan after the anneal treatments and are therefore, suitable for a quantitative interdiffusion analysis.

The θ/2θ x-ray diffraction scans for samples no. 918, 919, and 920 are shown (in Figs. 1-3) in the as-deposited condition (t=0) and after separate anneal intervals (t) of 7.20×10^3 sec (~2 hrs), 2.97×10^4 sec (~8 hrs), and 7.44×10^4 sec (~20 hrs). A superlattice Bragg reflection for the multilayer coating appears at a 2θ position of 44.10º with a spacing $d_{(hkl)}$ of 0.2052 ± 0.0004 nm that corresponds to a (111)fcc-(110)bcc growth. (Further electron diffraction analysis can reveal the specific growth-orientation relationship, as for example, if a Kurdjumov-Sachs epitaxial growth is found as seen in Au/Nb multilayers.[13]) The average multilayer-pair spacing $d_{Ni/CrMo}$ measured from the diffraction scans of all the as-deposited samples (t=0) are listed in Table 1. The $d_{Ni/CrMo}$ diffraction values are in agreement with the crystal microbalance measurements.

In general and with respect to the as-deposited conditions of each multilayer sample, the separation between the superlattice reflection and satellite peaks indicates an increase in the $d_{Ni/CrMo}$ after each anneal treatment. The diffraction measurements indicate an increase of up to 3% after 2-8 hrs and an increase of up to 9% after the 20 hr anneal treatment at 760 K. In addition, the Ni/CrMo superlattice reflection appears to split after the anneal treatments. The additional Bragg reflection(s) at 44.45º on the high angle side of the superlattice peak corresponds with the location of the Ni(111) and Cr(110) reflections indicating the occurrence of some phase separation, i.e. perhaps the relaxation of the superlattice to include strain free interplanar spacings. Also, note the simultaneous appearance and growth of a new reflection at 39.6º (from a diffuse to a well-defined peak in Figs. 1-3) as a result of the progressive anneal treatments. The corresponding interplanar spacing of 0.227 nm can be fitted to $Ni_2(Cr,Mo)$

intermetallic phases. The 0.227 nm spacings fits the (002) Bragg reflection of the tetragonal σ-phase with lattice parameters (a and c) of 0.880 nm and 0.454 nm, respectively as well as the (004) Bragg reflection of the orthorhombic P-phase with lattice parameters (a, b and c) of 1.698 nm, 0.475 nm and 0.907 nm, respectively.[5, 22] Since the measured superlattice spacing of the Ni/CrMo multilayer at 0.2052 nm is close to the (111) reflection and 0.2068 nm spacing observed for the solid solution of Ni(Cr,Mo), it's not readily apparent that a shift in this lattice parameter can be directly correlated to the onset of ordering.[23] However, the appearance of the intermetallic at 760 K in the present findings is in agreement with the onset of the intermetallic formation below 800 K as deduced from changes in the (111) spacing of long-range ordering for the Ni(Cr,Mo) solid solution.[23]

The amplification factor R(k) for each multilayer is determined from eqn (1). The decay of the integrated intensity of the satellite peaks (shown in Figs. 1-3) are plotted with the time of the anneal treatment. Ideally, the slope of the curves plotted in Fig. 4 equals 2R(k). However, a rapid non-linear decay of the satellite intensity is observed (in Fig. 4) after the 2 hr anneal treatment. This result is typical for short annealing times, i.e. less than 2 hrs, and has been attributed to several factors including recrystallization and grain growth that drive the early stages of annealing as well as the nonlinearity of the diffusion equation.[6, 24] Thus, the value for R(k) is determined using a linear regression fit to approximate the slope of the $\ln\{I^i(t)[I^i(0)]^{-1}\}$ vs time curves as plotted for $t \geq 2$ hrs. The curve fit introduces a statistical error for R(k). The dispersion relationship $B^2(h)$ can now be quantified for both (111) fcc and (110) bcc growth as given by eqn (3). The generalized interdiffusivity $\check{D}_B$ can then be computed from R(k) and $B^2(h)$ using eqn (2). The values of R(k), $B^2(h)$, and $\check{D}_B$ that are computed for the Ni/CrMo multilayer

samples are listed in Table 1. A plot of the $\check{D}_B$ vs $B^2(h)$ (shown in Fig. 5) can then be fit using eqn (8) to the polynomial expression

$$\check{D}_B = \check{D}\cdot[1 - 0.69B^2(h) + 0.14B^4(h)] \qquad (9)$$

The curve fit (shown in Fig. 5) to the Ni/CrMo data using the expression of eqn (9) yields a diffusion coefficient $\check{D}$ of $(15.24 \pm 2.68)\times10^{-20}$ $cm^2\cdot sec^{-1}$ for the Ni-CrMo system at 760 K. The value of $\check{D}$ for the Ni/CrMo system at 760 K is consistent with values obtained for other Ni alloy systems.[12] For comparison, a measured value for $\check{D}$ of $\sim3\times10^{-17}$ $cm^2\cdot sec^{-1}$ is reported for the $Ni_{0.40\text{-}0.47}Fe_{<0.07}Cu$ alloy at 760 K for both macroscopic and multilayer samples.[6, 12, 25] This value of $\check{D}$ should be and is much greater (by two orders of magnitude) than the value of $\check{D}$ expected and measured at 1.52×10^{-19} $cm^2\cdot sec^{-1}$ for the more refractory, Ni-(Cr,Mo) alloy system examined in this study.

5. Summary

The synthesis of Ni/CrMo multilayer structures by sputter deposition are used to measure the diffusion coefficient $\check{D}$ for the Ni-22wt.%Cr-13wt.%Mo, i.e. $Ni_2(Cr,Mo)$, alloy. This alloy has renewed interest for its corrosion resistance for long periods of time at low temperatures. The multilayer forms a metastable structure from which to directly measure diffusion coefficient(s) as a thermally controlled variant at low temperatures. A series of anneal treatment are used to promote interdiffusion between the (111) fcc Ni and (110) bcc $Cr_{0.65}Mo_{0.35}$ layers. The decay rate of this artificially induced short-range order is measured through x-ray diffraction and analyzed using the microscopic theory of diffusion. The value for the diffusion coefficient $\check{D}$ is computed as the long wavelength equivalent to a macroscopic diffusion couple. The diffusion coefficient is fit to the variation of the interdiffusion coefficients with the dispersion relationship for three Ni/CrMo multilayers, each with a different composition wavelength. A value for the diffusion coefficient $\check{D}$ of $(1.52 \pm 0.27)\times10^{-19}$ $cm^2 \cdot sec^{-1}$ is measured at 760 K. In addition, the x-ray diffraction indicates that a $Ni_2(Cr,Mo)$ intermetallic phase has evolved from the earliest stages at the 760 K anneal temperature.

Acknowledgments

This work was performed under the auspices of the U.S. Department of Energy by University of California, Lawrence Livermore National Laboratory under contract No. W-7405-Eng-48.

References

1. R.B. Leonard, Corrosion 25 (1969) 222.
2. F.G. Hodge, Corrosion 29 (1973) 375.
3. M. Raghavan, B.J. Berkowitz, and J.C. Scanlon, Metall. Mater. Trans. A 13 (1982) 979.
4. H.M. Tawancy, R.B. Herchenroeder and A.I. Asphahani, J. Metals 35 (1983) 37.
5. T.S.E. Summers, M.A. Wall, M. Kumar, S.J. Matthews, and R.B. Rebak, in Scientific Basis for Nuclear Waste Management XXII, Mater. Res. Soc. Symp. Proc. 556, eds. D.J. Wronkiewicz and J.H. Lee, (Materials Research Society, Warrendale, PA 1999) pp. 919-926.
6. T. Tsakalakos, Thins Solid Films 86 (1981) 79.
7. A.F. Jankowski and T. Tsakalakos, J. Appl. Phys. 57 (1985) 1835.
8. A.F. Jankowski, E.M. Sedillo, and J.P. Hayes, Jpn. J. Appl. Phys. 33 (1994) 5019.
9. A.G. Khachaturyan, Prog. Mater. Sci. 22 (1978) 1.
10. H.E. Cook, D. de Fontaine, and J.E. Hilliard, Acta Metall. 17 (1969) 765.
11. A.G. Khachaturyan, Theory of Structural Transformations in Solids, (John Wiley and Sons, New York 1983) pp. 128-136.
12. A.F. Jankowski and T. Tsakalakos, Metall. Trans. A 20 (1989) 357.
13. A.F. Jankowski and P.L. Perry, Thin Solid Films 193/194 (1990) 799.
14. R.E. Somekh, J. Vac. Sci. Technol. A 2 (1984) 1285.
15. W.D. Westwood, Mater. Res. Soc. Bull. 13(12) (1988) 46.
16. B.D. Cullity, Elements of X-Ray Difraction, (Addison-Wesley, Reading, MA 1978) pp. 512-521.
17. S.C. Moss, in Local Atomic Arrangements studied by X-Ray Diffraction, eds. J.B. Cohen and J.E. Hilliard (Gordon and Breach Science, New York, NY 1966) pp. 114-115.

18. J.W. Cahn, Acta Metall. 9 (1961) 795.

19. J.W. Cahn, Acta Metall. 10 (1962) 179.

20. J.W. Cahn and J.E. Hilliard, J. Chem. Phys. 28 (1958) 958.

21. H.E. Cook and J.E. Hilliard, J. Appl. Phys. 40 (1969) 2191.

22. P. Villars and L.C. Calvert, in Pearson's Handbook of Crystallographic Data for Intermetallic Phases, Vol. 1 (American Society for Metals, Metals Park, OH 1985).

23. L. Karmazin, Mater. Sci. Eng'g. 54 (1982) 247.

24. T. Tsakalakos, Scripta Metall. 20 (1986) 471.

25. R. Poerschke, W. Wagner, and H. Wolenberger, J. Phys. F: Met. Phys. 16 (1986) 421.

Tables

Table I. Parameters of the Ni/CrMo multilayers

No.	ω (sec^{-1})	N	$d_{Ni/CrMo}$ (nm)		Γ_{Ni}	2R(k) (10^{-5} sec^{-1})	$B^2(h)$ (nm^{-2})	$\check{D}_B$ (10^{-20} $cm^2 \cdot sec^{-1}$)
			crystal	x-ray				
918	0.050	300	3.27	3.29 ± .08	0.633	-3.05 ± 0.08	3.60	4.24 ± 0.10
919	0.033	200	4.76	4.99 ± .17	0.637	-1.20 ± 0.30	1.58	3.79 ± 0.95
920	0.020	120	7.90	8.10 ± .14	0.624	-1.16 ± 0.23	0.60	9.67 ± 1.93

Figure Captions

Figure 1. A plot of the log peak-intensity of x-ray reflections versus 2θ position for the Ni/CrMo multilayer sample no. 918 reveals the superlattice reflection surrounded by satellite peaks. The satellite peak intensities decrease with the time of the anneal treatment.

Figure 2. A plot of the log peak-intensity of x-ray reflections versus 2θ position for the Ni/CrMo multilayer sample no. 919 reveals the superlattice reflection surrounded by satellite peaks. The satellite peak intensities decrease with the time of the anneal treatment.

Figure 3. A plot of the log peak-intensity of x-ray reflections versus 2θ position for the Ni/CrMo multilayer sample no. 920 reveals the superlattice reflection surrounded by satellite peaks. The satellite peak intensities decrease with the time of the anneal treatment.

Figure 4. A plot of $\ln\{I^i(t)\cdot[I^i(0)]^{-1}\}$ versus the time (t) of annealing at 760 K reveals the decay in the amplitude of the –1 and +1 satellite reflections, i.e. composition fluctuation, in the Ni/CrMo multilayer samples no. 918, 919, and 920.

Figure 5. A plot of the interdiffusivity coefficient $\check{D}_B$ versus the dispersion relationship $B^2(h)$ for the Ni/CrMo multilayer samples.

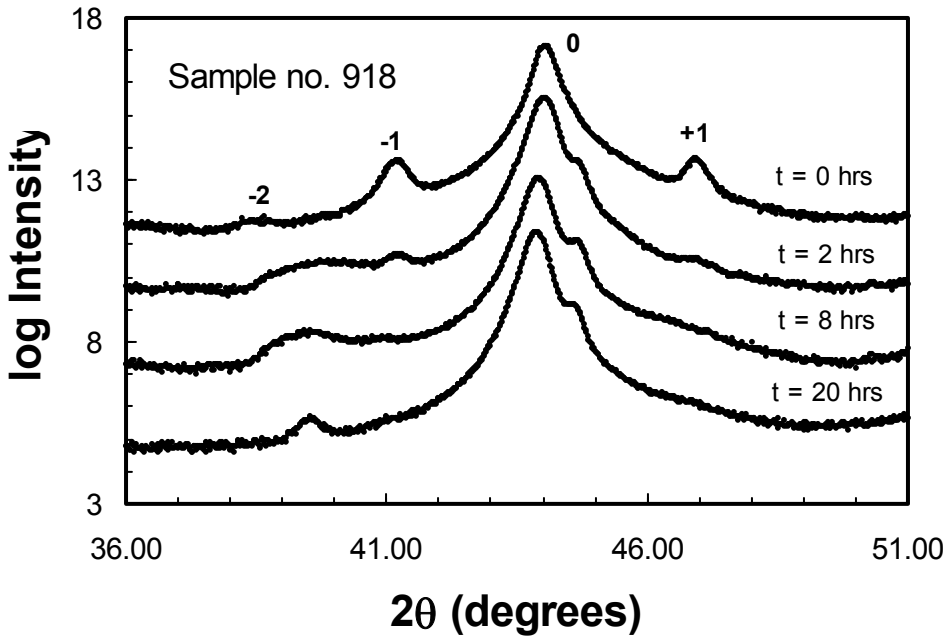
Sample no. 918
log Intensity
2θ (degrees)
18
13
8
3
36.00
41.00
46.00
51.00
-2
-1
0
+1
t = 0 hrs
t = 2 hrs
t = 8 hrs
t = 20 hrs

Figure 1.

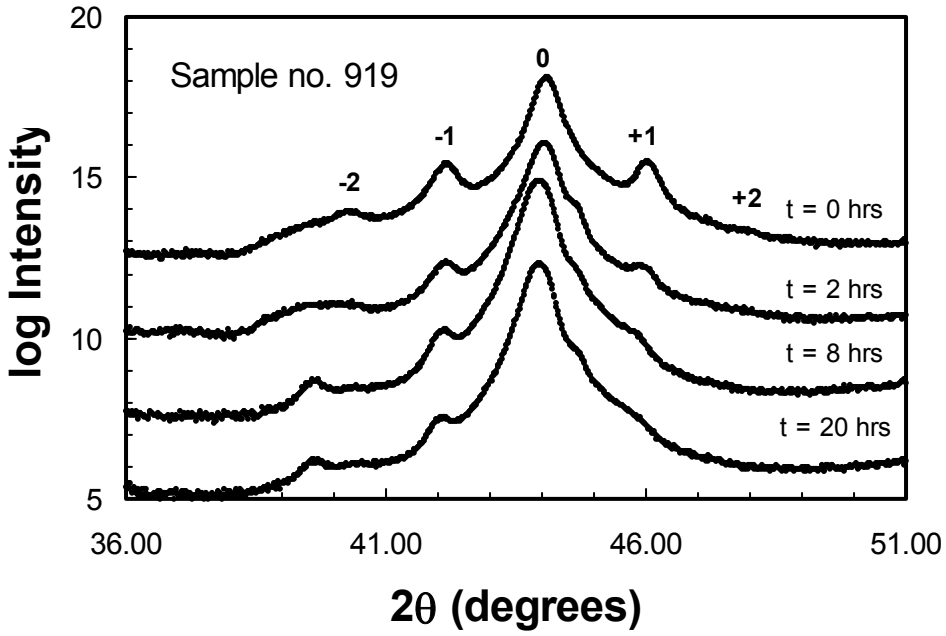
Sample no. 919
0
-1
+1
-2
+2
t = 0 hrs
t = 2 hrs
t = 8 hrs
t = 20 hrs
log Intensity
20
15
10
5
36.00
41.00
46.00
51.00
2θ (degrees)

Figure 2.

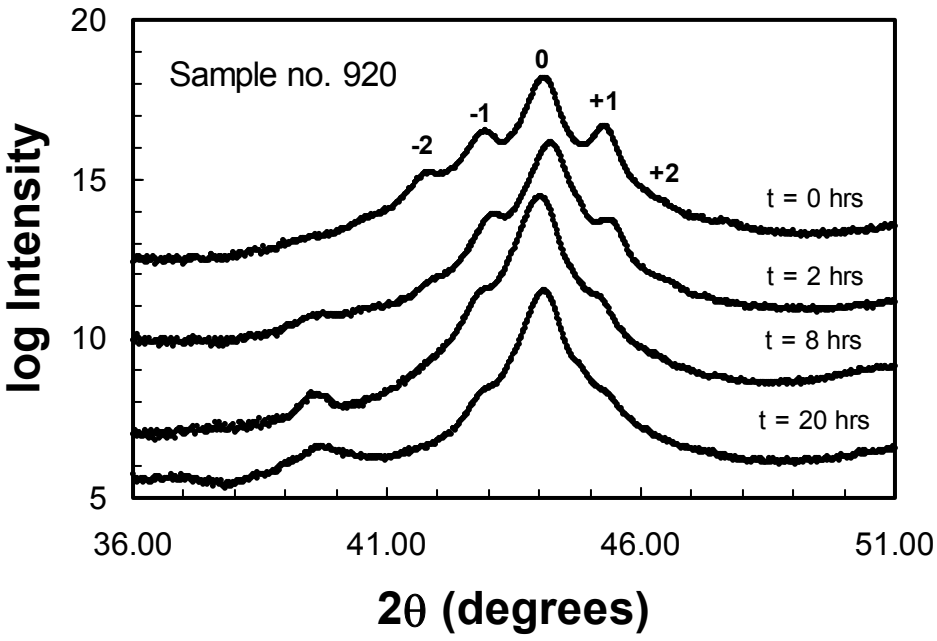
Sample no. 920
0
-1
+1
-2
+2
t = 0 hrs
t = 2 hrs
t = 8 hrs
t = 20 hrs
log Intensity
20
15
10
5
36.00
41.00
46.00
51.00
2θ (degrees)

Figure 3.

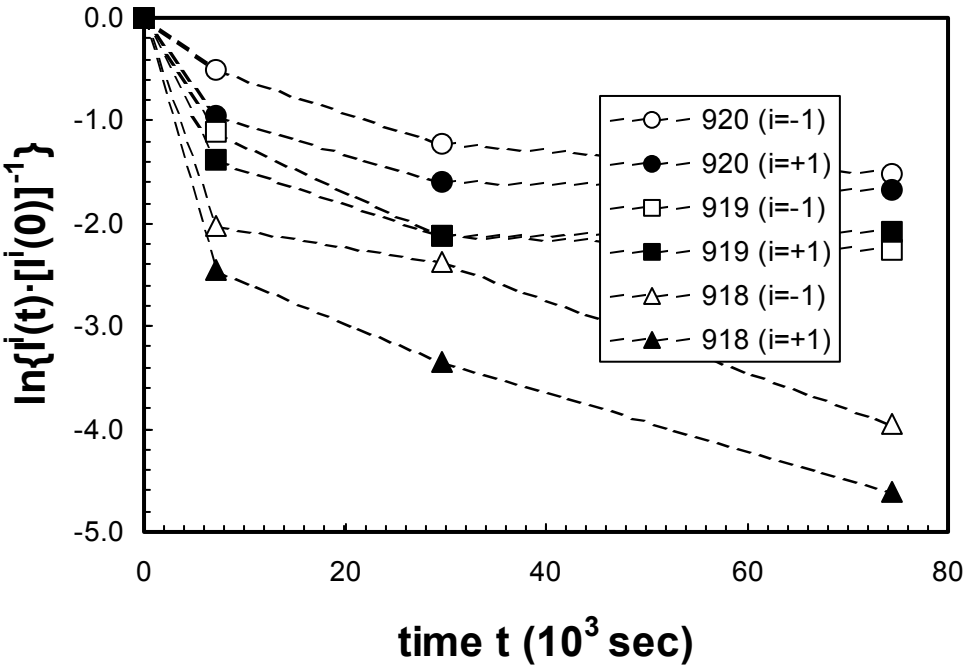
0.0
-1.0
-2.0
-3.0
-4.0
-5.0
0
20
40
60
80
ln{I^i(t)·[I^i(0)]^-1}
time t (10^3 sec)
920 (i=-1)
920 (i=+1)
919 (i=-1)
919 (i=+1)
918 (i=-1)
918 (i=+1)

Figure 4.

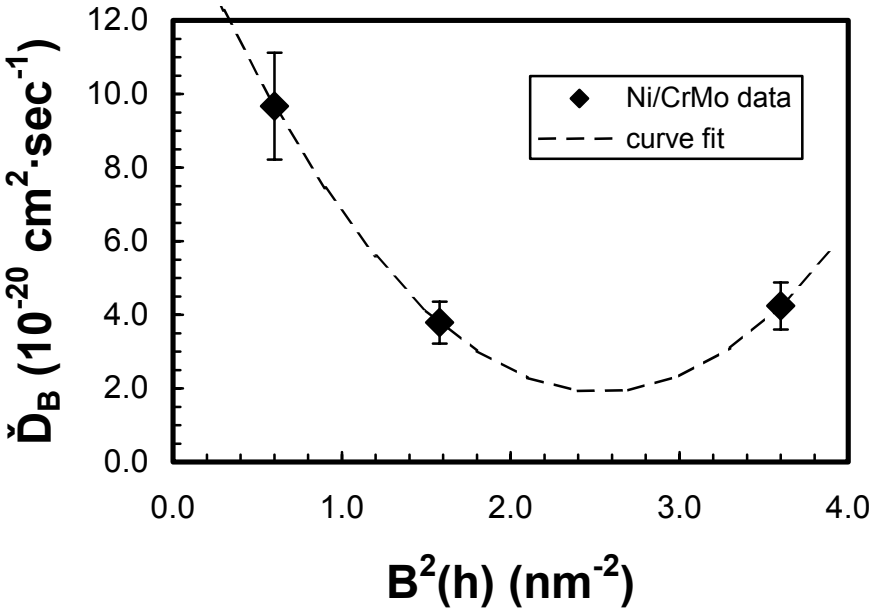
12.0
10.0
8.0
6.0
4.0
2.0
0.0
0.0
1.0
2.0
3.0
4.0
Ni/CrMo data
curve fit
$\check{D}_B$ (10^{-20} cm^2.sec^{-1})
$B^2(h)$ (nm^{-2})

Figure 5.